Attenuation and reflection of radio waves by a melting layer of precipitation

Klaassen, W.

Published in:
IEE Proceedings. Part H: Microwaves, Antennas and Propagation

DOI:
10.1049/ip-h-2.1990.0007

Publication date:
1990

Attenuation and reflection of radio waves by a melting layer of precipitation

W. Klaassen, PhD

Indexing terms: Radio wave propagation (tropospheric)

Abstract: Attenuation and reflection of a melting layer are calculated using a meteorological model. The model employs a new scheme for the calculation of the dielectric properties of melting ice particles with densities ranging from those of loose snow to hail, and a new scheme for calculating the melting rate is employed. The input parameters are derived from high resolution Doppler radar data and provide a data set for statistical analysis. Statistical relations were derived for attenuation in the melting layer based on measurements made with a surface rain gauge, a radar (with and without a polarisation facility), and a lower frequency satellite link. It was found that the specific attenuation of melting snow surpasses the value of rain because of the larger size and particle number density during melting, the attenuation within the melting layer increasing with its reflection. In stratiform precipitation, the attenuation in the melting layer is found to increase only slightly with frequency. The reflection in the melting layer decreases with the frequency of the radio waves in such a way that a bright band is only observed for frequencies below 20 GHz.

1 Introduction

Statistical information about the attenuation of satellite communication signals by precipitation is useful in the development of systems. This attenuation is primarily ascribed to rain, but Leitao and Watson [14] and Kozu *et al.* [13] demonstrate the significance of a melting layer. The main problem of including a melting layer in simulation studies was that the processes which occur during melting were poorly understood. For instance, as an explanation of the high reflection in the melting layer, it was assumed that melted water remained outside the snowflake and formed a shell around it (Dissanayake and McEwan [5]), or an extreme amount of aggregation and breakup had to be assumed to fit the calculated and observed reflection during melting (Lhermitte and Atlas [16]).

A more realistic way of explaining the high radar reflection of melting snow is to assume that the particle is a heterogeneous mixture of ice, liquid water and air with the melted water surrounding the individual ice crystals (Klaassen [11]). This model also explains the varying ratio between the reflection in and below the melting layer from the snowflake mass density and the vertical extent from the air temperature profile.

To use this melting layer model for attenuation studies, several input parameters, such as the mean snowflake size and mass density, must be determined. These parameters are found by fitting the model results to high resolution Doppler radar measurements. As several independent parameters influence the attenuation, the results are presented statistically.

The main features of the model and the data set are described, the attenuation statistics are given and the implications discussed.

Paper 7043H (E11), first received 18th April and in revised form 27th September 1989

The author was with the Department of Electrical Engineering, Delft University of Technology, PO Box 5031, 2600 GA Delft, The Netherlands, and is now with the Department of Physical Geography, University of Groningen, Kerklaan 30, 9751 NN Haren, The Netherlands

2 The melting layer model

The model has been described by Klaassen [11]. Only those features that are necessary to understand the results on propagation will be discussed here. The main assumptions are:

(*a*) The attenuation and reflection are calculated for spherical particles using Mie theory. Measurements with polarisation radar (Hall *et al.* [7], Hendry *et al.* [8]) clearly show horizontal flattening of the particles towards the end of melting and this phenomenon could be included in the model when the shape and angle distributions of these particles are better known.

(*b*) The model is one-dimensional and stationary; starting with only frozen particles above the 0°C level, the melting and scattering are calculated in small descending height steps.

2.1 The dielectric constant of a melting particle

The average dielectric constant of a melting particle is calculated from the Maxwell–Garnett theory of inclusions in a matrix. The theory has been extended by Bohren and Battan [2] to elliptical inclusions, giving:

$$\varepsilon_{av} = \frac{(1-f_i)\varepsilon_m + f_i\beta}{1-f_i+f_i\beta} \tag{1}$$

$$\beta = \frac{2\varepsilon_m}{\varepsilon_i-\varepsilon_m}\left[\frac{\varepsilon_i}{\varepsilon_i-\varepsilon_m} C\log(\varepsilon_i/\varepsilon_m) - 1\right]$$

where ε_{av} is the dielectric constant of the mixture, ε_m the dielectric constant of the matrix, ε_i the dielectric constant of the inclusions and f_i the volume fraction of the inclusions; C log is the complex logarithm.

Eqn. 1 is valid for a mixture of two components; melting snow consists of three components: ice, water and air. The dielectric constant of the three-component mixture has been calculated from eqn. 1, in two steps: first the dielectric constant of the ice–water mixture is

calculated and then the wet ice–air mixture. In the first step water is taken as the matrix after Bohren and Battan [2], and in agreement with the observations of Fujiyoshi [6], assuming that the water forms a film around the ice crystals during most of the melting stages. In the second step wet ice is taken as the matrix because the scattering results from wet ice and the ice crystals are interconnected within the flake. It appears essential to take wet ice as the matrix in order to find high reflection and attenuation values during melting.

2.2 The size and mass density of melting particles

The attenuation due to dry snowflakes is very low and the level of reflection is mainly determined by the melted diameter (the diameter of the resulting drop when all ice is melted, Cumming [4]). For melting snow the density must also be taken into account, as reflection and attenuation depend on the volume expansion of the melt water. Instead of using just one size and density, a complete range is modelled to fit the observations more realistically. Additionally, a range damps out the consequences of electrical resonance in individual particles. The model starts with a gamma distribution of melted sizes:

$$N(D) = N_0 D^2 \exp[-5.67D/D_o] \quad (2)$$

where D is the melted particle size (mm), N the particle number concentration ($mm^{-1} m^{-3}$), D_o ($= 5.67/\Lambda$) the median particle size (mm), and N_0 a constant.

During melting, the particle size distribution may change because of: (*a*) variations in fall velocity, (*b*) aggregation and breakup and (*c*) condensation of water vapour.

(*a*) Assuming the mass flux of precipitation particles is constant with height, results in a particle number concentration inversely proportional to the fall velocity. According to Lhermitte and Atlas [16] the Doppler fall velocity in stratiform precipitation increases from 2 to 6 m/s during melting, resulting in a decrease by a factor of 3 in the particle number concentration or 5 dB in reflection. Together with changes in the dielectric constant, the change in fall velocity is the other main factor causing the high reflection in the melting layer relative to rain.

(*b*) Aggregation is the mechanism by which snowflakes are formed from individual ice crystals in the upper part of a cloud. In a melting layer, aggregation is less important because of the small vertical extent of this layer. Spontaneous breakup in the later stages of melting has been observed using filter paper on a mountain slope, Yokoyama *et al.* [25], an optical spectrometer in an aircraft, Stewart *et al.* [23], a two wavelength radar, Yokoyama *et al.* [24], and using snowflake structure analysis, Fujiyoshi [6]. Breakup in hail is only observed for extremely large stones, Rasmussen *et al.* [21]. To find agreement with these observations, it is assumed that breakup only occurs for loose particles. The limit for breakup is set for particles with a dry mass density below 0.2 g cm^{-3}. The time for breakup is set when 80% of the particle mass is melted, as Fujiyoshi [6] found the largest fragments near the end of melting. Three fragments are assumed with 87, 11.4 and 1.6% of the initial mass after Brazier-Smith *et al.* [3]. As the observations on breakup during melting are restricted, one simulation is performed without breakup to analyse the influence of breakup.

(*c*) Most of the melting heat is received from the latent heat of the condensation of water vapour on the flake. This results in an increase of about 10% in water mass and precipitation intensity during melting.

The mass density of a melting particle is calculated using the dry density and assuming a linear decrease of particle volume with melted fraction, until the particle is completely saturated with water.

The dry density of loose snowflakes is modelled with the observations of Magano and Nakamura [18]. The main problem is that the dry density may range from between 0.005 g cm^{-3} for loose snow to 0.9 g cm^{-3} for hail. Therefore the dry density is taken as a free parameter in the model. The dry density strongly influences the simulated reflection and fall velocity during melting: with a dry density of 0.005 g cm^{-3} the calculated maximum reflection during melting appears to be of a factor 100 beyond the value for a melting hail stone of the same mass, and thus, the dry density can easily be determined from the radar observations.

The disadvantage of including another parameter in the model is the deficiency of direct relations between the attenuation or reflection in the melting layer and the rain intensity. This problem is solved in the paper by determining statistical relations.

By taking the dry density as a free parameter in the model, the variable radar brightness of the melting layer is realistically explained. The bright band disappears in convective clouds, where upward winds lift cloud droplets or even rain drops to heights above the 0°C level. After lifting, the droplets can collide with snow flakes to form graupel, and rain drops refreeze to form hail stones. During melting, the large mass density of these particles reduces the volume expansion of melt water and the resulting reflection.

According to this theory, the attenuation above the melting layer is no longer negligible in situations without a bright band. In this situation, the wet and compact ice particles show reflection and attenuation similar to that of rain drops of the same mass. So it seems realistic to estimate the attenuation in convective situations from that of rain, up to the height above the expected 0°C level where radar reflection decreases significantly, and to restrict the melting layer model to bright band situations.

2.3 The melting rate

The melting rate depends on the air temperature and humidity. The air is assumed to be saturated with water vapour within a cloud. The air temperature is often assumed to decrease linearly with height in the melting layer, but this is a poor assumption as the melting results in cooling of the air. As an alternative, the model determines the air temperature from the energy balance of the rising air. This results in an almost isothermal layer in the upper part of the melting layer and a slow start of melting. Consequently the melting particles remain in the first stage of melting for longer. During this stage the particles and their attenuation are still large.

To determine the air temperature, the model requires the mean vertical air velocity as an input parameter. This parameter is determined from the Doppler spectra of a vertically scanning radar. In situations with a distinct radar bright band, the mean vertical air velocity V_a was found to be highly correlated with the reflectivity in rain Z_r, according to Klaassen [11]:

$$V_a = 0.011 Z_r^{0.4} \quad (3)$$

where Z_r is the reflection in the rain just below the melting layer ($mm^6 m^{-3}$) and V_a is expressed in (m/s). Eqn. 3 is recommended when Doppler information about the bright band is lacking.

3 Observations

Measurements for the statistical analysis were obtained using the Delft Atmospheric Research Radar (DARR), as described by Ligthart and Nieuwkerk [17]. The characteristics of this high resolution FM-CW radar during the measurements are given in Table 1:

Table 1: Radar characteristics

Centre frequency	3.315 GHz (λ = 9 cm)
Scanning direction	vertical
Range resolution	30 m
Doppler velocity resolution	0.56 m/s

In 1983, over three hours of observation were made in precipitation that showed the melting layer as a distinct radar bright band. From these observations, a data set of 50 measurements each of one minute duration was selected to represent the full range of reflection values observed just below the melting region. As the statistical results of this study are dependent on these observations, the most important observations from Klaassen [11] will be reproduced here.

A main parameter of the melting layer is the maximum reflectivity excess Z_{xm}, defined as the ratio of the maximum reflection in the melting layer to that of the underlying rain. In Fig. 1, this ratio is shown as a function of the reflection in rain Z_r. Note that Z_r = 23 dBz can be associated with a rain intensity of 1 mm/hr and Z_r = 44 dBz with that of 20 mm/hr, indicating the range of rain intensities observed. A rain intensity of 20 mm/hr is very high for stratiform precipitation and this observation may be exceptional. During light precipitation, aggregation is restricted and the resulting compact ice particles restrict the value of Z_{xm}. At intermediate rain intensities all values of Z_{xm} up to 15 dB appear.

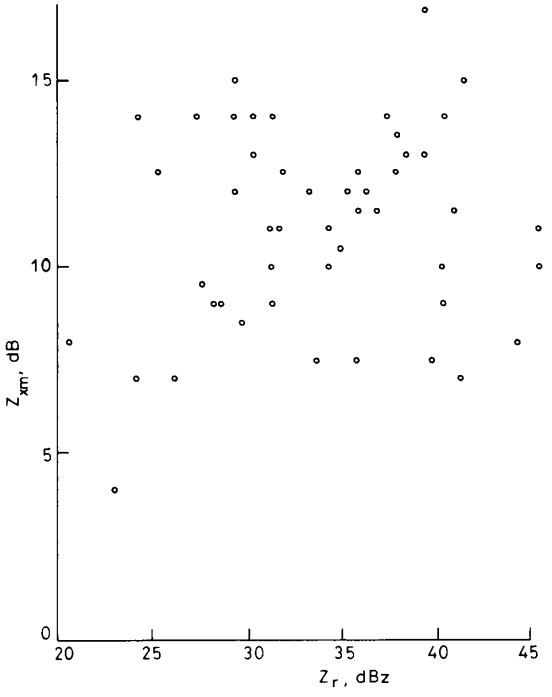

Fig. 1 *Maximum reflectivity excess in the melting layer vs. reflection in the rain just below the melting layer, as measured with the DARR in 1983 during precipitation with a distinct bright band*

The thickness of the bright band, defined by Klaassen [11] and closely related to the vertical extent of the region in which increased reflection occurs, appears to be highly correlated with Z_r (Fig. 2). Consequently, it is not necessary to measure the vertical extent of the bright band as an individual parameter. This is advantageous, as a high resolution radar and a careful interpretation method are required in order to measure the boundaries accurately. According to the model, the increase of the bright band thickness with precipitation intensity is primarily caused by a larger isothermal layer on the top of the melting layer and to a lesser extent by an increase of the mean particle mass. This increase of the isothermal layer with precipitation intensity is in agreement with the observations of Matsuo [19].

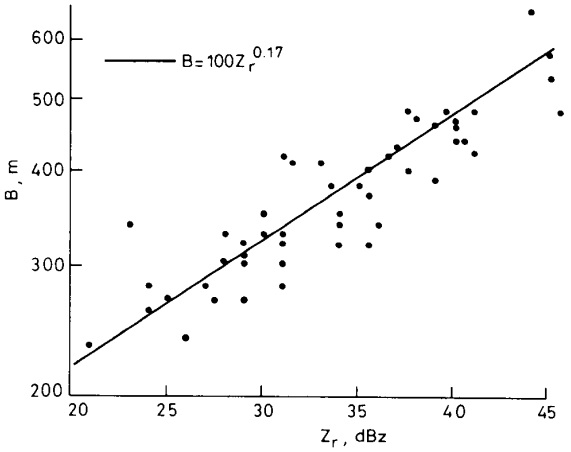

Fig. 2 *Vertical thickness of the bright band for the same observations as used for Fig. 1*

4 Results

Attenuation has been calculated for frequencies of 12, 20 and 30 GHz, close to the frequency bands that will be used in the Olympus satellite. Statistical relations are given for the complete data set, initially some vertical profiles are analysed that are calculated for an almost average situation in order to establish the sensitivity of the model.

4.1 Vertical profiles of attenuation and reflection

Fig. 3 shows the specific attenuation (SA) increasing in the bright band; when compared to the value in rain this increase is most marked for low radio frequencies. An increase by a factor of 3 in SA is explained by the lower fall velocity and larger resulting particle number density in the first stage of melting. At 30 GHZ the effects of SA enhancement by a larger particle size and reduction by the restricted amount of liquid water appear compensatory in most stages of melting. At 12 GHz the enhancement is stronger as scattering is closer to the Raleigh value.

Fig. 3 shows that breakup influences the attenuation significantly, implying that the amount of breakup should be accurately estimated. Breakup results in smaller particles, so the mass of the melting particles before breakup exceeds the mass of the resulting raindrops. The heavier particles in the melting layer reflect radar waves much more effectively, so the observed reflection is simulated with a smaller particle number density that results in less attenuation for the situation with breakup.

The vertical profile of SA at 30 GHz is in rough agreement with the calculations of Jain and Watson [9] at

36 GHz; Kharadly and Choi [10] also find the maximum attenuation in the upper part of the bright band, but their value is much larger due to a different simulation method employed.

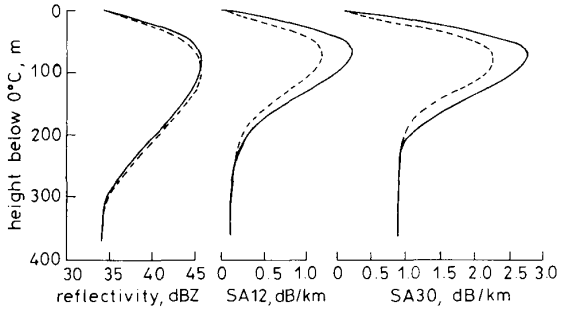

Fig. 3 *Vertical profiles of reflection and specific attenuation in the melting layer*

- - - - basic model
——— model without breakup

Fig. 4 shows similar reflection profiles at 1 and 3 GHz as the wavelengths are long compared with the scattering particles, the Rayleigh approximation still holds. The reflection decreases for higher frequencies, initially in the upper region of the melting layer where the particle dimensions are large. A radar bright band is simulated

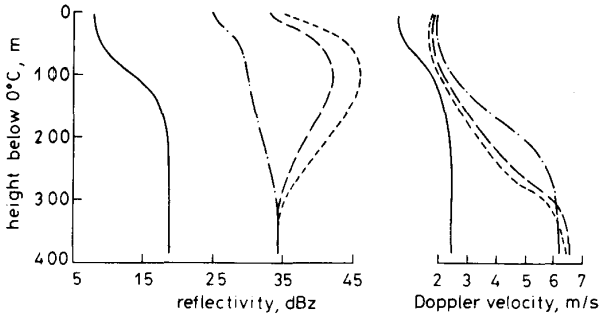

Fig. 4 *Vertical profiles of reflection and Doppler velocity within the melting layer vs. radar frequency*

- - - - 1 and 3 GHz, — — 10 GHz, —·— 30 GHz, ——— 100 GHz

only for frequencies below 20 GHz, so the reflectivity peak is found to disappear at lower frequencies than the *SA* peak. The reflection in rain is found to decrease for frequencies above 30 GHz, especially for large drops. This change in reflection is primarily caused by deviations from Raleigh scattering; a minor influence being the frequency dependence of the dielectric constants of ice and water. The profile at 100 GHz is mainly sensitive to small particles that require only a small height interval for melting. The simulated change in reflection and Doppler velocity at 100 GHz appears to be in good agreement with the observations of Lhermitte [15] at 94 GHz, although a correction for the finite dimensions of ice crystals should be included at these frequencies, Sadiku [22].

The Doppler velocity is calculated for a vertical wind of 0.3 m/s and shows a shift from the fall velocity of snow to the value in rain. The height of this transition increases with frequency, due to decreasing sensitivity of the reflection to large particles.

4.2 Statistical relations for the attenuation

The suitability of different measurable parameters for calculation of the attenuation excess in the melting layer is determined on the basis of a statistical analysis. This analysis is performed assuming high quality observations of:

(*a*) the rain intensity at the earth's surface,

(*b*) the reflection in rain and the maximum reflectivity excess in the melting layer, and

(*c*) the reflection in orthogonal polarisations of rain and the maximum reflectivity excess in the melting layer.

The results are expressed in the following form:

$$\begin{aligned} A_e(F) &= \alpha R^{\beta} && \pm\sigma_1 \\ A_e(F) &= \delta Z_r^{\phi} Z_{xm}^{\psi} && \pm\sigma_2 \\ A_e(F) &= \zeta Z_r^{\nu} Z_{xm}^{\mu} Z_{dr}^{\eta} && \pm\sigma_3 \end{aligned} \tag{4}$$

where $A_e(F)$ is the attenuation excess (dB) of the melting layer at radio frequency F (GHz), R the rain intensity (mm/hr), $\alpha - \eta$ statistical constants, σ the rms scatter and Z_{dr} the ratio between the reflection at horizontal and vertical polarisation in the rain. The attenuation excess is defined as the difference between the total attenuation in the melting layer and the attenuation of an equal path length in rain with the drop size distribution that results from melting. The total path attenuation is found by assuming rain up to the 0°C level and adding the attenuation excess of the melting layer. Z_{dr} has been calculated assuming Prupacher–Pitter [20] rain drop shapes. A maximum value of Z_{dr} was often observed in the lower part of the bright band, but when using eqn. 4 the value of Z_{dr} and Z_r immediately below the bright band should be used.

The constants in eqn. 4 were derived assuming Z_r, Z_{xm} and Z_{dr} expressed in their usual dimensions and not dB. The constants were derived by minimising the resulting scatter, but unity powers are preferred when they only slightly reduce accuracy. To find a minimum absolute scatter the power law fit was made directly, as shown in Figs. 5–7. The results for the constants of eqn. 4 given in Table 2.

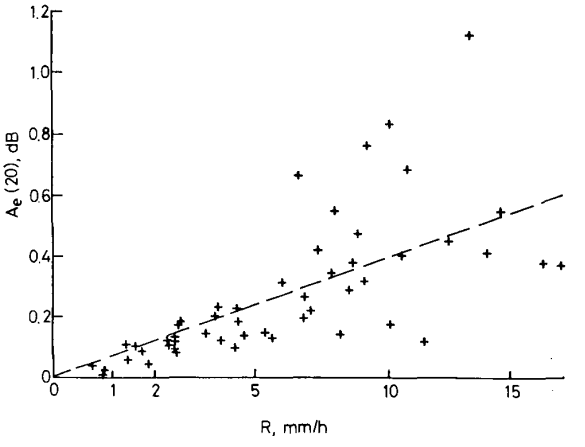

Fig. 5 *Attenuation excess of the bright band vs. rain intensity*

- - - $A_e(20) = 0.0707R^{0.75}$

The attenuation excess can only be reasonably approximated using the rain intensity (Fig. 5). When using a surface rain gauge, the accuracy further deteriorates because of vertical variations in the rain intensity.

A smaller scatter is obtained when the reflection of the melting layer is taken into account (Fig. 6). The attenuation excess appears to be proportional to the maximum reflectivity excess in the melting layer.

The differential reflectivity in rain gives a good indication of the particle sizes and leads to a further improve-

ment in the estimation of the attenuation excess (Fig. 7). A high power of Z_{dr} is found, showing that the attenuation excess is very sensitive to the mean particle size. The high power law of Z_{dr} implies that this quantity must be accurately measured. The values of the power law,

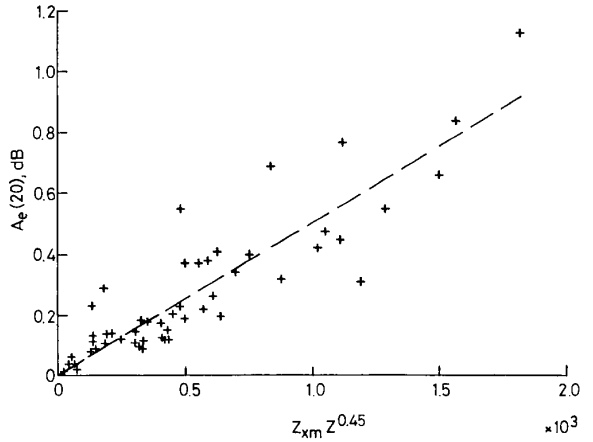

Fig. 6 *Attenuation excess vs. radar reflection in, and below the bright band*

— — $A_e(20) = 502 \times 10^{-6}\, ZZ_{xm}^{0.45}$

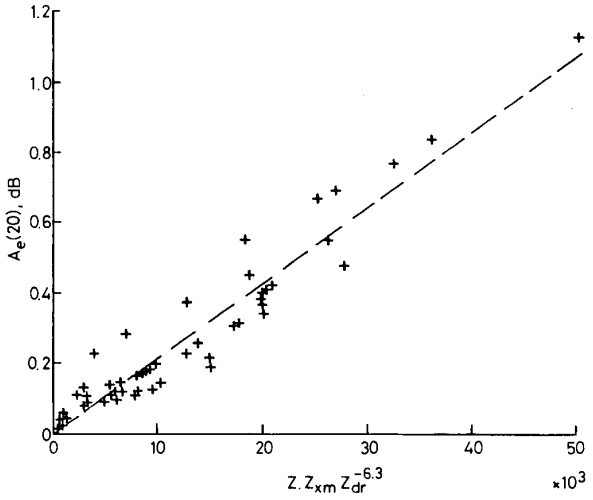

Fig. 7 *Attenuation excess vs. directional reflectivity radar measurements*

— — $A_e(20) = 21.3 \times 10^{-6}\, ZZ_{xm}\,Z_{dr}^{-6.3}$

Table 2: Statistical relations for the attenuation excess

F (GHz)	12	20	30
α	0.0456	0.0707	0.0733
β	0.85	0.75	0.65
σ_1 (dB)	0.130	0.167	0.176
δ ($\times 10^{-6}$)	258	502	553
ϕ	0.50	0.45	0.42
ψ	1	1	1
σ_2 (dB)	0.077	0.106	0.105
ζ ($\times 10^{-6}$)	13.9	21.3	20.0
ν	1	1	1
μ	1	1	1
η	−5.5	−6.3	−6.7
σ_3 (dB)	0.049	0.064	0.076

given in Table 2, are similar to the value of the relation between the rain intensity and differential reflectivity measurements given by Klaassen [12]

$$R = 0.0068 Z_r Z_{dr}^{-6.2} \quad (5)$$

showing that when Z_{dr} can be measured with sufficient accuracy to determine the rain intensity, this measurement can also be used to estimate the attenuation excess in the melting layer.

The attenuation on a satellite path can also be estimated from measurements on an existing link at a lower frequency. The ratio $A(G)/A(F)$ of the attenuation at frequencies G and F is calculated for rain with and without a melting layer above the rain. The influence of including a melting layer on $A(G)/A(F)$ is analysed by assuming the 0°C level at a height of 2 km. When the 0°C level is higher, the relative influence of the melting layer decreases and vice versa.

The results for $A(20)/A(12)$ and $A(30)/A(20)$ are shown in Figs. 8 and 9. The result for $A(30)/A(20)$ is in good

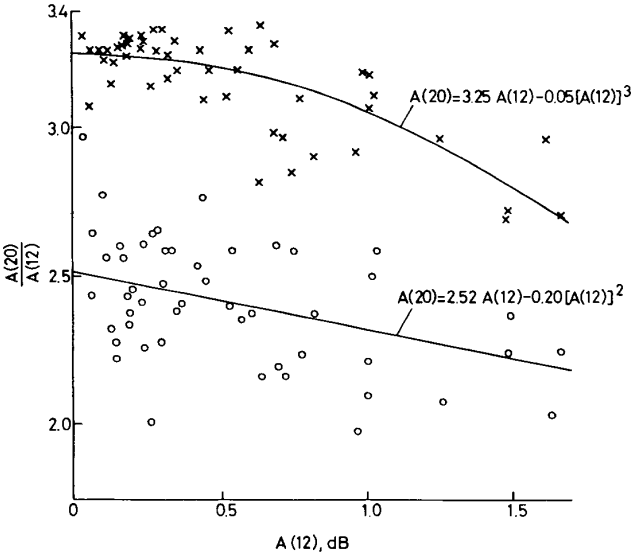

Fig. 8 *Ratio of satellite path attenuation at 20 and 12 GHz against path attenuation at vertical propagation at 12 GHz*

× rain only
○ rain plus melting layer

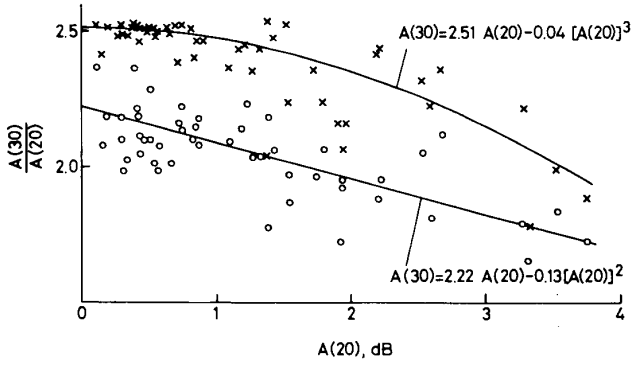

Fig. 9 *Ratio of satellite path attenuation at 30 and 20 GHz against path attenuation at vertical propagation at 20 GHz*

× rain only
○ rain plus melting layer

agreement with observations of Kozu *et al.* [13] and Andrews *et al.* [1]. The simulations show a similar result for $A(20)/A(12)$. For small $A(F)$ with rain the results approach the Raleigh theory. The decrease of $A(G)/A(F)$ with $A(F)$ and with inclusion of a melting layer are caused by increasing deviations of the scattering of larger particles and smaller wavelengths from this approximation. Note that $A(F)$ is calculated for vertical propagation and a 0°C level at 2 km, while $A(G)/A(F)$ is

basically independent of the elevation angle. It is hazardous to extrapolate the results of Figs. 8 and 9 to larger values of $A(F)$, as melting layers are less probable for stronger rains, and $A(G)/A(F)$ is expected to slowly approach the value of unity for higher $A(F)$.

In Section 2.2 it is proposed that showers without a bright band can be examined with the 'rain only' curve. The bright band is a common feature in horizontally extended stratiform precipitation and the absence of a bright band is characteristic of showers with restricted dimensions. Assuming more than one ground station, the showers can be bypassed using site diversity, so the bright band situation is preferential for use in the design of new telecommunication satellites.

5 Conclusion

The main conclusion of this study is that when a radar bright band is present the attenuation of a satellite link is proportionately less with respect to frequency. Consequently less extra power is required to maintain a link at a higher frequency.

The attenuation of a satellite link can be estimated from surface measurements of rain intensity or radar reflection. According to the simulations, it appears advantageous to measure the reflection for the estimation of the attenuation in the melting layer. By using radar, the height of the melting layer and variations in rain intensity along the satellite path can also be detected. Including differential reflectivity measurements may result in an even more accurate estimation of the path attenuation.

When using radar for observations of the melting layer, it appears advantageous to use a long wavelength (>5 cm). For long wavelengths the scattering approaches the results of the Raleigh theory, yielding a reflectivity excess in the melting layer that is independent of wavelength whereas for shorter waves this reflectivity excess disappears.

The results are calculated with a state-of-the-art meteorological model and appear to be in good agreement with the available measurements. Further verification is planned after the launch of the Olympus satellite.

6 Acknowledgments

The study was funded by the Netherlands Organization for Scientific Research (NWO) and initiated by Professor L.P. Ligthart. Helpful discussions with Prof. G. Brussaard (Eindhoven University), H.W.J. Russchenberg and the corrections of J.B. Zaat-Jones are gratefully acknowledged.

7 References

1 ANDREWS, J.H., OZBAY, C., PRATT, T., BOSTIAN, C.W., MANUS, E.A., GAINES, J.M., MARSHALL, R.E., STUTZMAN, W.L., and WILEY, P.H.: 'Results of the VPI&SU COMSTAR experiment', *Rad. Sci.*, 1982, **17,** pp. 1349–1359
2 BOHREN, C.F., and BATTAN, L.J.: 'Radar backscatter by spongy ice spheres', *J. Atmos. Sci.*, 1982, **39,** pp. 2623–2629
3 BRAZIER-SMITH, P.R., JENNINGS, S.G., and LATHAM, J.: 'Raindrop interactions and rainfall rates within clouds', *Quart. J. Roy. Meteor. Soc.*, 1973, **99,** pp. 260–272
4 CUMMING, W.A.: 'The dielectric properties of ice and snow at 3.2 cm', *J. Appl. Phys.*, 1952, **23,** p. 768
5 DISSANAYAKE, A.W., and McEWAN, N.J.: 'Radar and attenuation properties of rain and bright band', *IEE Conf. Publ.*, 1978, **169-2,** pp. 125–129
6 FUJIYOSHI, Y.: 'Melting snowflakes', *J. Atmos. Sci.*, **43,** pp. 307–311
7 HALL, M.P.M., GODDARD, J.W.F., and CHERRY, S.M.: 'Identification of hydrometeors and other targets by dual-polarization radar', *Rad. Sci.*, 1984, **19,** pp. 132–140
8 HENDRY, A., ANTAR, Y.M.M., and McCORMICK, G.C.: 'On the relationship between the degree of preferred orientation in precipitation and dual-polarisation radar echo characteristics', *Rad. Sci.*, 1987, **22,** pp. 37–50
9 JAIN, Y.M., and WATSON, P.A.: 'Attenuation in melting snow on microwave and millimeter-wave terrestrial radio links', *Electron. Lett.*, 1985, **21,** (2), pp. 68–69
10 KHARADLY, M.M.Z., and CHOI, A.S.V.: 'A simplified approach to the evaluation of EMW propagation characteristics in rain and melting snow', *IEEE Trans.*, 1988, **AP 36-2,** pp. 282–296
11 KLAASSEN, W.: 'Radar observations and simulation of the melting layer of precipitation', *J. Atmos. Sci.*, 1988, **45,** pp. 3741–3753
12 KLAASSEN, W.: 'Determination of rain intensity from Doppler spectra of vertically scanning radar', *J. Atmos. Oceanic Techn.*, 1989, **6,** pp. 552–562
13 KOZU, T., AWAKA, J., FUKUCHI, H., and NAKAMURA, K.: 'Rain attenuation ratios on 30/20 and 14/12 GHz satellite to earth paths', *Rad. Sci.*, 1988, **23,** pp. 409–418
14 LEITAO, M.J., and WATSON, P.A.: 'Method for prediction of attenuation on earth–space links based on radar measurements of the physical structure of rainfall', *IEE Proc. F*, 1986, **133,** pp. 429–440
15 LHERMITTE, R.M.: 'Cloud and precipitation remote sensing at 94 GHz', *IEEE Trans.*, 1988, **GE-26,** pp. 207–216
16 LHERMITTE, R.M., and ATLAS, D.: 'Doppler fall speed and particle growth in stratiform precipitation'. Proc. 10th Radar Weather Conf., 1963, pp. 297–302
17 LIGTHART, L.P., and NIEUWKERK, L.R.: 'FM-CW Delft atmospheric research radar', *IEE Proc. F*, 1980, **127,** pp. 421–426
18 MAGANO, C., and NAKAMURA, T.: 'Aerodynamic studies of falling snowflakes', *J. Meteor. Soc. Japan*, 1965, **43,** pp. 139–147
19 MATSUO, T.: 'Melting of snowflakes in the atmosphere', *Proc. 9th Int. Cloud Physics Conf.*, 1984, Ac. Sci. Estonian SSR, pp. 279–281
20 PRUPPACHER, H.R., and PITTER, R.L.: 'A semi-empirical determination of the shape of cloud and rain drops', *J. Atmos. Sci.*, 1971, **28,** pp. 86–94
21 RASMUSSEN, R.M., LEVIZZANI, V., and PRUPPACHER, H.R.: 'A wind tunnel and theoretical study on the melting behaviour of atmospheric ice particles of radius >500 mm', *J. Atmos. Sci.*, **41,** pp. 381–388
22 SADIKU, M.N.O.: 'Refractive index of snow at microwave frequencies', *Appl. Opt.*, 1985, **24,** pp. 572–575
23 STEWART, R.E., MARWITZ, J.D., PACE, J.C., and CARBONE, R.E.: 'Characteristics through the melting layer of stratiform clouds', *J. Atmos. Sci.*, 1984, **22,** pp. 3227–3237
24 YOKOYAMA, T., TANAKA, H., NAKAMURA, K., and AWAKA, J.: 'Microphysical processes of melting snowflakes detected by two wavelength radar', *J. Meteor. Soc. Japan*, 1984, **62,** pp. 668–677
25 YOKOYAMA, T., TANAKA, H., AKAEDA, K., OHTANI, T., YOSHIZAWA, N., YAMANAKA, M.D., MITA, A., ISHIZAKA, Y., and ONO, A.: 'Observations on microphysical processes in the stratiform precipitations including melting layers at Mt. Fuji', *J. Meteor. Soc. Japan*, 1985, **63,** pp. 100–111